LOCAL SIGNALING FROM A RETINAL PROSTHETIC IN A RODENT RETINITIS PIGMENTOSA MODEL *IN VIVO*

James W. Fransen[1], **Gobinda Pangeni**[2], **Machelle T. Pardue**[3,4], and **Maureen A. McCall**[1,2,*]

[1]University of Louisville, Department of Anatomical Sciences and Neurobiology 40202

[2]University of Louisville, Department of Ophthalmology & Visual Sciences, 301 E. Muhammad Ali Blvd Room 420, Louisville, KY 40202

[3]Emory University, Department of Ophthalmology, 30322

[4]Atlanta VA Medical Center, Rehab R&D Center of Excellence, 30033

Abstract

Objective—In clinical trials, retinitis pigmentosa (RP) patients implanted with a retinal prosthetic device show enhanced spatial vision, including the ability to read large text and navigate. New prosthetics aim to increase spatial resolution by decreasing pixel/electrode size and limiting current spread. To examine spatial resolution of a new prosthetic design, we characterized and compared two photovoltaic array (PVA) designs and their interaction with the retina after subretinal implantation in transgenic S334ter line 3 rats (Tg S334ter-3).

Approach—PVAs were implanted subretinally at two stages of degeneration and assessed *in vivo* using extracellular recordings in the superior colliculus (SC). Several aspects of this interaction were evaluated by varying duration, irradiance and position of a near infrared (NIR) laser focused on the PVA. These characteristics included: activation threshold, response linearity, SC signal topography and spatial localization. The major design difference between the two PVA designs is the inclusion of local current returns in the newer design.

Main Results—When tested *in vivo*, PVA-evoked response thresholds were independent of pixel/electrode size, but differ between the new and old PVA designs. Response thresholds were independent of implantation age and duration (7.5 months). For both prosthesis designs, threshold intensities were within established safety limits. PVA-evoked responses require inner retina synaptic transmission and do not directly activate retinal ganglion cells (RGCs). The new PVA design evokes local retinal activation, which is not found with the older PVA design that lacks local current returns.

Significance—Our study provides *in vivo* evidence that prosthetics make functional contacts with the inner nuclear layer at several stages of degeneration. The new PVA design enhances local activation within the retina and SC. Together these results predict that the new design can potentially harness the inherent processing within the retina and is likely to produce higher spatial resolution in patients.

*Correspondence Address: 301 E. Muhammad Ali Blvd, Louisville, KY 40202, mo.mccall@louisville.edu, Phone: 502-852-3386.
Disclosures: The authors declare no competing financial interests.

Keywords

retina; prosthesis; photovoltaic; retinitis pigmentosa; artificial vision

INTRODUCTION

Many blinding eye diseases result from photoreceptor dysfunction or degeneration (Hartong et al. 2006; Ambati and Fowler 2012). The most prevalent of these diseases are age related macular degeneration (AMD) and RP, which together affect ~1.9 million people in the United States alone (Friedman et al. 2004). While photoreceptors are lost in RP, much of the inner retinal cells and circuitry are preserved until late in the degenerative process (Jones et al. 2003).

In the absence of photoreceptor input, electrical currents can be used to activate the remaining retinal neurons and elicit the perception of phosphenes (Gebhard 1952; Kurosawa 1954; Humayun et al. 1999; Humayun et al. 2003; Chow et al. 2004). In animal models of RP, direct electrical stimulation of the retina evokes spiking activity even when light evoked RGC responses are absent (O'Hearn et al. 2006; Jensen and Rizzo 2008; Sekirnjak et al. 2009; Margalit et al. 2011). In the Royal College of Surgeons (RCS) rat RP model, stimulation of a subretinally implanted monopolar photovoltaic array (mPVA) evoked responses in the SC, a central target of RGC axons (DeMarco et al. 2007). Clinical trials in human RP patients show that stimulation of implanted prosthetics restores visual perception, including the ability to read large text and navigate the environment (Chow et al 2004; Zrenner et al. 2011; Humayun et al. 2012).

Depending on the design, prosthetic devices can be implanted either sub- or epiretinally. An epiretinal prosthesis is placed on the nerve fiber layer/RGC side and directly stimulates RGCs, their axons, and potentially other cells in the INL as well. In contrast, a subretinal prosthesis is placed between the outer retina and the retinal pigment epithelium. Activation thresholds for stimulation appear similar for subretinal and epiretinal stimulation (O'Hearn et al. 2006; Shah et al. 2006; Shyu et al. 2006) indicating that each is equally safe. Depending on current spread, multiple retinal layers may be stimulated with either design but ideally, a prosthesis will stimulate only one layer of cells. If current spread is limited to one layer, the subretinal design has the advantage that stimulation of bipolar cells will maintain signaling in the inner retina, allowing the signal to be processed within the retinal circuitry. This should enhance spatial localization and reduce the difficulty of subsequent signaling in more central visual targets and the interpretation of visual percepts. In contrast, epiretinal prosthetics bypass the processing power of the inner retinal circuitry. In addition, an epiretinal design has to contend with stimulating not only the RGCs but also axons that course across to the retina toward the optic nerve head. This is likely to obscure the location of the signal and generate poorly localized visual percepts.

To recreate useful, high-resolution visual perception, critical prosthetic design considerations include: (1) reducing electrode size to minimize current spread and increase spatial resolution; (2) creating a predictable relationship between prosthetic stimulation and the subsequent retinal response to modulate RGC output; (3) maintaining a stable prosthesis-

retina interface during disease progression and (4) keeping current levels below safety limits to reduce the possibility of damaging the retina or device (Butterwick et al. 2007). Currently, prosthetic devices in clinical trials address safety issues but have been limited in their ability to provide high spatial resolution (Chow et al. 2010; Stingl et al. 2013; Humayun et al. 2012). To address these requirements and attempt to increase spatial resolution, a next generation bipolar PVA (bPVA) has been designed to limit current spread across the device. It was first tested *in vitro,* where stimulation with near infrared (NIR) light evoked repeatable RGC responses with a latency of 10–70 ms (Wang et al. 2012; Mathieson et al. 2012). An initial test *in vivo* showed that a NIR stimulus evoked cortical potentials (Mandel et al. 2013).

Here we evaluate and compare several aspects of the interface between the retina and both monopolar and bipolar PVAs, using our established *in vivo* recording assay (DeMarco et al. 2007) in the SC of the Tg S334ter-3 rat RP model. The results present a comprehensive assessment of the characteristics of the PVA-evoked response in the SC. We demonstrate that PVA stimulation produces reliable responses that are well below established safety limits. The response generated by both PVAs produce a reliable retinal representation in the SC, but only the bPVA produces local retinal activation in the SC. Finally, we show that this activation is achieved via bPVA interaction with the INL and without direct stimulation of RGCs.

METHODS

Animals

All experimental procedures were conducted in accordance with regulations described in the Statement for the Use of Animals in Ophthalmic and Visual Research and with the approval of the Institutuional Animal Care and Use Committee of the University of Louisville. Homozygous Tg S334ter-3 rats (a gift of Dr. Matthew LaVail, University of California, San Francisco) were bred to Long Evans pigmented rats to create pigmented hemizygous Tg S334ter-3 rats, which were used for all experiments. In addition to native rhodopsin, their photoreceptors express a truncated rhodopsin protein that induces rod photoreceptor degeneration beginning at about P6 (http://ucsfeye.net/mlavailRDratmodels.shtml; Chen et al. 1995; Concepcion et al. 2002; McGill et al. 2012). For Tg S334ter-3 rats implanted with mPVAs we compared responses at two implantation ages (P35 or P75) and two post-surgery duration ranges (50–90 or 120–150 days). Rats were implanted with bPVAs at approximately the same ages (P45 and P75) and were tested after similar postsurgery durations. Because thresholds for response were similar across all conditions (shown in Figure 4 for mPVAs), the results from all implantation groups were combined following this anlysis. In Tg S334ter-3 rats implanted with bPVAs, our comparison of responses included data from all implantation ages and durations.

Prosthetic Devices

The mPVA (previously refered to as the ASR, see Chow et al. 2004) was provided by Optobionics, Inc (Naperville, IL). Its fabrication and use have been previously described (Chow et al. 2001; Pardue et al. 2001; Pardue et al. 2005; DeMarco et al. 2007). In short, the

mPVA (Figure 1A, 1C) is a 20 μm thick solid silicon chip with a 1 mm diameter. The array has a light-reactive side, comprising ~1200, 25 × 25 μm elements (pixels). Each pixel contains a photodiode connected to a 10μm diameter activated iridium oxide electrode. Current produced by the photodiodes returns to a single ground return on the opposite face of the array. Each pixel operates independently, converting incident light into a cathodic first, bi-phasic charge-balanced pulse.

The design and fabrication of the bPVA (provided by D. Palanker, Stanford University; Figure 1B) has also been described previously (Loudin et al. 2011; Wang et al. 2012; Mathieson et al. 2012). Dimensions of the bPVA are 0.8 mm wide × 1.2 mm length × 30 μm thick and there are three versions, each with a different pixel size (280, 140, or 70 μm). Regardless of size, each pixel contains a central electrode, whose size varies proportionally with pixel size. The pixel is surrounded by three photodiodes in series, fabricated on a silicon wafer with 5 μm trenches separating adjacent pixels. Each pixel contains its own return electrode and current flows between the center and return electrodes. The size of the return electrode also is proportional to pixel size. When stimulus irradiance is fixed and within the linear range of current output, larger pixels collect more light and produce larger currents at the expense of lower resolution compared to smaller pixels. At high irradiance levels, a logarithmic range of current output occurs and it is possible that the current produced across pixel size will be more similar. Similar to mPVA devices, bPVA electrodes are coated in iridium oxide and generate cathodic first, bi-phasic charge-balanced electrical pulses (Cogan 2008). Both designs are sensitive in the near infrared range (880 – 915 nm), wavelengths where rat photoreceptors are insensitive (Jacobs et al. 2001).

Implant Surgery

Details of the sterile implantation surgery have been published previously (Chow et al. 2001; Pardue et al. 2005; DeMarco et al. 2007). Briefly, a surgical plane of anesthesia was attained with ketamine/xylazine (80/10 mg/kg), administered by intraperitoneal injection. Once anesthetized, a topical analgesic was applied to the right eye (proparacaine, 0.5%, Alcon). The pupil was dilated with tropicamide and phenylephrine (1% and 2.5% respectively, Bausch and Lomb). Then a suture was placed in the upper eyelid and traction applied to expose the superior portion of the eye. A second suture in the superior conjunctiva was used to rotate the eye forward. After a small area of the conjunctiva was removed to expose the sclera, a 19-gauge vitrectomy knife was used to make an ~1mm incision through the sclera and retina. After 10 minutes, the retina naturally detached from the RPE and the prosthetic device was inserted into the retinotomy site between the retina and RPE. Subretinal placement was verified by direct observation using a rat fundus lens (Ocular Instruments). The retinotomy incision was left to heal on its own, with no health complications observed in any implanted rat. Devices were implanted at either 35–45 or 75 days of age. At these ages, significant declines in photoreceptor number, ERG b-wave and OKT are already evident (McGill et al. 2012).

Two to four weeks after implantation, device placement was verified and an evaluation of the surgical outcome was performed using three techniques: fundus imaging, spectral domain optical coherence tomography (SD-OCT) and fluorescein angiography. Rats were

anesthetized and the pupil dilated as described above. A clear, non-corrective contact lens was placed on the eye to prevent desiccation. A montage of the retina, including the optic nerve head and the PVA *in situ*, was collected using a Spectralis OCT (Heidelberg Engineering). Images were used to look for surgical complications including edema and retinal tear. In addition, the montage was used to determine the location of the PVA relative to the optic nerve head when both could be imaged together. Fluorescein angiography was performed immediately following OCT imaging. Rats were injected intraperitoneally with a 10% solution of AK-Fluor (75 mg/kg; Akorn Inc, Lake Forest, IL) and images of the retinal vasculature overlying the PVA were captured within 3–5 minutes post-injection.

Surgical preparation for extracellular recording

Animals were initially anesthetized as decribed above for implantation surgery and a custom catheter was placed in the femoral vein. For the remainder of the experiment, the ketamine/ xylazine mixture (diluted 1:1 in Ringer's solution) was administered continuously into the femoral vein, using an infusion pump (~0.35 mL/hr). The anesthetized animal was placed in a stereotaxic and a craniotomy was made (~1.5 mm diameter) centered between the lambdoidal and coronal sutures on the left side of the skull. The overlying cortex was aspirated and the left SC was directly viewed under a dissecting microscope.

Prosthetic and retinal stimulation

A PASCAL (Medical Laser Systems Topcon) photocoagulation laser was modified and provided by D. Palanker and J. Loudin, Stanford University. The laser produced either a near infrared (NIR, 905 nm) or a green (visible, 535 nm) spot that was focused onto the PVA. The visible spot was used for alignment onto the PVA and also to stimulate the long/ medium wavelength sensitive cone photoreceptors. To record visually evoked SC responses, the visible laser irradiance was held constant at 44.6 μW/mm^2 as was the pulse duration held constant at 4 ms. The wavelength of the NIR stimulus selectively stimulated the PVA, as rat photoreceptors insensitive to this wavelength (DeMarco et al. 2007) and rats implanted with a PVA that lack visible-evoked SC responses responded to NIR stimulation. For most experiments, the laser spot covered a surface area of 0.785 mm^2 (1.0 mm diameter) and filled the majority of the PVA surface area (0.785 mm^2 and 0.96 mm^2 for mPVAs and bPVAs, respectively).

Topographic mapping in the SC—To map the PVA-evoked responses across the SC, a 1.0 mm diameter NIR spot with an irradiance of 8.0 mW/mm^2 was centered on the PVA and pulsed for 4 ms at 1 Hz. The recording electrode was systematically moved across the SC (see "*In vivo* SC recordings" below).

Irradiance/duration threshold experiments—To determine thresholds for stimulation, a 1.0 mm spot was centered on the PVA and NIR laser irradiance was varied in discreet steps (2.4, 5.1, 8.0, 11.6, 17.1, or 20.1 mW/mm^2) at 7 pulse widths (0.25, 0.5, 1, 2, 4, 10, and 20 ms). Pulse width, irradiance and the number of presentations were controlled via custom software (programmed in LabView; National Instruments Corporation). If responses were above threshold (defined in Methods: SC Response and Data Analysis) at the lowest irradiance, neutral density filters were used to reduce the irradiance to 10%, 5%, or 0.5% of

the original irradiance. After the stimulation threshold at one pulse duration was established, pulse duration was increased and threshold determined at the new pulse duration. We compared the mean threshold response between conditions at each pulse duration using either t-tests (with Welch's correction) for normally distributed responses or the Mann-Whitney U test when the responses were not normally distributed.

Local retinal activation experiments—To evaluate the spatial extent of retinal activation in the SC, a small diameter NIR spot (0.5 mm) with an irradiance of 32 mW/mm^2 was centered on the PVA and pulsed for 4 ms at 1 Hz. This resulted in a stimulated area of 0.196 mm^2, which is 25% of the mPVA and 20% of the bPVA.

In vivo SC recordings

Multicellular extracellular activity was recorded in the SC of Tg S334ter-3 rats implanted with either an bPVA or mPVA, as described previously (Woch et al. 2001; Sagdullaev et al. (2003); DeMarco et al. 2007). Spontaneous and evoked activity was recorded using custom-made, lacquer coated tungsten electrodes (0.25–2 MΩ). Responses were recorded and digitized at 21 kHz (Power1401, CED, UK), and stored for offline analyses. The NIR and visible evoked responses were analyzed (Spike2, CED, UK). Spike rates were obtained from recorded responses and averaged into 50 ms bins.

SC Response Topography—To map the PVA-evoked response, we systematically moved the position of the electrode at regular intervals (200 μm between recording sites), starting at the medial-caudal end and ending at the lateral-rostral end, resulting in up to 54 recording sites. To ensure that the superficial SC layers (which receive direct RGC axon input) were sampled, the depth of the recording was restricted to the upper 150–400 μm of the SC. At each recorded location we presented 20–25 stimulus repeats with the NIR laser centered on the PVA. During these experiments, an SC site with a robust PVA response was found and responses at that that site were used to characterize the response, define stimulation thresholds, evaluate local SC activation or compare NIR and visual stimulation.

Suprathreshold duration and irradiance response function—To determine the relationship between SC response and pulse duration, responses were recorded at a fixed laser irradiance (11.6 mw/mm^2) while pulse duration was varied (0.25, 0.5, 1, 2, 4, 10 and 20 ms). Similarly, to determine the relationship between SC response and stimulus irradiance, responses were recorded at a fixed pulse duration (4 ms), while irradiance was varied (2.4, 5.1, 8.0, 11.6, 17.1, and 20.1 mW/mm^2). For both, the average peak response was plotted as a function of laser pulse duration (or irradiance). To examine if these stimuli produced significant changes across the range tested, the average response at each stimulus was compared to the response to the maximal stimulus using a One-way ANOVA followed by Bonferoni posthoc comparisons.

Extent of local retinal activation in the SC—To examine the spatial extent of implant-evoked responses, a 0.5 mm diameter spot was presented across the PVA in five distinct regions with little overlap. These locations are shown in a schematic diagram (Figure 8). This approach had two advantages. First, it provided precise control over the position of the

stimulus on the PVA. Second, this limited the number of electrode penetrations and avoided uneccesary damage to the SC, which could result in an artificial decline in responses. Because the response variability across the surface of the device is independent from animal to animal, we had to evaluate each animal individually rather than average the responses from multiple animals. To characterize the spatial extent of these responses for an individual animal, the average peak response for each region was computed and the standard error based on trial to trial variability was measured. The averages for the five regions were then compared using a One-way ANOVA followed by Bonferroni's post hoc test.

Pharmacologic Manipulation of Inner Retinal Synaptic Transmission

To distinguish between direct stimulation of RGCs and indirect stimulation of RGCs through the inner retina, INL to RGC transmission was blocked using excitatory and inhibitory blockers. If responses are still present after blocking synaptic transmission, this would indicate RGCs are being directly stimulated. If no responses remain after blocking synaptic transmission, we can conclude that the INL is stimulated without involving RGCs directly. We compared untreated PVA-evoked responses to those evoked after intravitreal injection of saline (2.5μl) and to PVA-stimulation 3–5 min after intravitreal injection of synaptic blockers (2.5μl). The synaptic blocker cocktail consisted of two glutamate receptor antagonists (DAP-5 (50 μM) and CNQX (10 μM), Sigma-Aldrich) and three inhibitory receptor antagonists (picrotoxin 10 μM, TPMPA 50 μM, strychnine 10 μM; Sigma-Aldrich) dissolved in lactated Ringer's solution. These concentrations represent the final concentrations in the vitreous and were calculated using the estimated vitreal volume for the rat eye (52.5 μl; Sha and Kwong 2006). A complete block of synaptic signaling was characterized by a complete or nearly complete decline in spontaneous activity within 5 minutes of synaptic blocker injection.

SC Response and Data Analyses

A significant response was defined as activity that rose 3 standard deviations (SD) above spontaneous activity. Peak firing rate was determined by subtracting the spontaneous activity (in Hz) from the peak response of the post stimulus time histogram (PSTH). The start of evoked activity was defined as the time at which activity reached the 3 SD threshold; the end of evoked activity was defined as the time at which activity returned below the 3 SD threshold. Time to peak was defined as the time from the stimulus onset to the peak of the PSTH trace. Response duration was calculated by subtracting the start time from the end time of the evoked activity. In experiments in which we defined the threshold for stimulation, a response was defined as evoked activity that rose 3 SDs above spontaneous activity in at least 50% of the stimulus presentations.

Statistics were calculated using the analysis software Prism (V5.04; Graphpad Software, La Jolla, CA). Exact statistical analyses are described in the sections above. Normality of the data was assessed using a Kolmogorov-Smirnov test. Normally distributed data were analyzed with parametric statistics (t-test or One-way ANOVA followed by a Bonferroni post hoc test). Non-normally distributed data were analyzed with non-parametric statistics (Kruskal-Wallis one-way rank analysis followed by Dunn's multiple comparison post hoc test). Figure error bars plot ± the standard error of the mean.

Results

Retinal and vascular integrity are maintained in implanted Tg S334ter-3 rats

Using fundus photography, SD-OCT and fluorsecein angiography, we evaluated the retinal integrity of Tg S334ter-3 rats implanted with an mPVA or bPVA. Fundus images confirmed the subretinal position of devices in all animals, which were typically superior to the optic nerve head (ONH; Figures 1Ai & Aii). Fluorescein angiograms (Figure 1B) showed that the retinal vasculature over and adjacent to the PVA were similar and blood vessels showed no leakage. OCT imaging confirmed that most devices were succesfully implanted (25/31 bPVA and 21/25 mPVA) in the subretinal space in close proximity to the retina (Figure 1C). The remainder showed retinal tears (Figure 1D) or other unresolved surgical complications, but none showed any signs of infection or rejection of the PVA. Animals with poor surgical outcomes were excluded from the functional assessments that follow.

PVA-evoked responses are robust and topographically localized across the dorsal surface of the SC

NIR stimulation of PVAs evoked SC responses (referred to hereafter as PVA-evoked responses; Figure 2B) in almost every Tg S334ter-3 rat successfully implanted with an mPVA (n = 21/25) or bPVA (n=20/21) device. Success rates were independent of the age at implantation or duration of implantation.

We determined the PVA retinal location and completely mapped PVA-evoked responses in the SC of 11 rats with mPVAs and 12 with bPVAs. Because the SC is retinotopically organized, the relationship between the PVA's retinal location and SC activation should be predictable. To determine if this relationship was consistent across animals, we characterized the topographic organization of the PVA-evoked responses across the surface of the SC. SC activation across animals had similar spatial profiles (Figure 2B), with each having a central area with very robust responses (2B; dark red on the heat map) and response amplitude fell off with distance from the center until PVA-evoked responses were no longer present. We plotted and compared the centers of the retinal location based on the fundus images (Figure 2A & 2C) to the center of PVA-evoked activity on the SC maps (Figures 2D). When all the centers of activation and retinal locations were plotted, we observed a consistent spatial relationship of PVA-evoked response location in the SC (Drager and Hubel 1976) with retinal topographic location in 20/23 rats (indicated by the single headed arrows). The other three rats (indicated by red letters in Figure 2C & D) showed a discrepancy between the location of the PVA in the OCT image and the location of SC activity. We speculate that this might have occurred because the PVA location in the retina drifted between the time of fundus imaging and SC recording.

The retina-PVA interface is independent of implantation age and duration

At P35, there is a significant reduction in photoreceptor nuclei in the ONL of unimplanted Tg S334ter-3 rats (Sagdullaev et al. 2003; McGill et al. 2012). By P75, the ONL contains only a single layer of photoreceptor nuclei. We used these two time points (P35 and P75) to evaluate the ability to establish a retina-PVA interface because they represent different stages of degeneration. We measured the threshold for stimulation and used it as a measure

of the retina-PVA interface first in rats with mPVAs. Within the range of irradiance that we could test (20.1mW/mm^2), response thresholds were only significantly higher for pulse durations of 0.5 and 1 ms in rats implanted with an mPVA at P75 (Figure 3A; t-test with Welch's correction, *p<0.05).

To determine how well the retina-PVA interface is maintained during the degenerative process, we implanted rats at P75 and measured the threshold for stimulation 50–90 or for 120–150 days later. In rats implanted for 50 – 90 days, the shortest pulse duration did not produce responses above threshold even at our highest irradiance stimulus. Across the range of irradiance that we tested, we found no other significant difference between thresholds for these two implantation durations. We conclude that over a reasonably wide range of parameters, thresholds are independent of implant age or duration and a PVA/retina interface can be maintained in rats as old as 225 days (Figure 3B). It is possible that at short implantation durations that the retina-PVA interface is not fully established, resulting in a lack of responses at the shortest pulse duration. Finally, regardless of experimental condition, all thresholds were well below established safety limits.

PVA-evoked response threshold is similar across bPVA pixel size but bPVA thresholds are higher than mPVA

A reduction in pixel size should enhance spatial coding but at the cost of a decrease in the light collection area and the current output, possibly leading to an increase in the irradiance required to reach threshold. When we compared the three bPVA pixel diameters, threshold was similar (Figure 4A; small (70 μm, n = 5), medium (140 μm, n = 6) or large (280 μm, n = 6)) and well below established safety limits (approximately 50 fold lower). When the two devices designs were compared, thresholds for mPVAs were signficantly lower than bPVAs (Figure 4B), except at the shortest pulse durations (0.5 ms; Mann-Whitney U test: ***p<0.001, ****p<0.0001). This may reflect a greater current spread in the mPVA due to its lack of local current return electrodes.

Latency and duration of the bPVA and mPVA-evoked responses differ from one another and from visually evoked responses

When the latency and duration for the two PVA designs were compared, the time to peak of mPVA-evoked responses was significantly shorter than bPVA-evoked responses (Figure 5D; mPVA: 42.62 ±2.19 ms; bPVA: 52.78 ±2.93 ms; Kruskal-Wallis p<0.0001; Dunn's post hoc: *p<0.05). Similarly, mPVA-evoked responses had shorter response durations (Figure 5E; mPVA: 71.2 ±18.49 ms; bPVA: 124.5 ± 27.3 ms; Kruskal-Wallis p<0.0001; Dunn's post hoc: **p<0.01). This difference in time to peak is consistent with the difference in threshold; to the same irradiance the mPVA should create a larger excitatory drive and evoke a faster response compared to the bPVA. This does not explain the difference in duration and is something that will need further exploration.

Tg S334ter-3 rats with either mPVAs or bPVAs retain visually evoked responses up to 180 days of age (single responses shown in Figure 5B compared to single PVA-evoked responses in 5A). Visually evoked responses had significantly slower time to peak than PVA-evoked responses (Figure 5C and D; 176 ±6.88 ms; Dunn's post hoc: **p<0.01,

***p<0.001) and significantly longer response durations (Figure 5E; visually evoked: 354.5 ±40.3ms; Dunn's post hoc: **p<0.01, ***p<0.001). The shorter time to peak in the PVA-evoked response is consistent with bypassing part of the retinal signaling cascade, which includes the photoreceptor transduction cascade and glutamatergic signaling to the bipolar cells. The difference in duration likely is due to the separation between ON and OFF RGC responses during visible stimulation that would not be present during PVA stimulation.

PVA-evoked responses in the SC result from direct PVA stimulation of the INL

The rapid time to peak of the PVA response is consistent with bypassing some of the retinal circuit. To differentiate between direct PVA stimulation of the INL or ganglion cells, we examined PVA-evoked responses in the same eyes before and after elimination of synaptic transmission in the retina. Spontaneous and bPVA-evoked responses were similar prior to and after a control injection of 2.5 μl saline (Figure 6A, B, D). In the same eyes, a subsequent injection of saline solution containing inhibitory and excitatory blockers (also 2.5 μl; 50 μM DAP-5, 10 μM CNQX, 10 μM picrotoxin, 50 μM TPMPA and 10 μM strychnine) eliminated both spontaneous and bPVA-evoked responses (Figure 6C, D). This result shows that current from the bPVA activates the cells of the inner retina and their synaptic output is required to stimulate RGCs and evoke SC responses.

The dynamic range of PVA- evoked responses

In WT retina, photoreceptor output and RGC spiking rate are proportional to light intensity and stimulus duration within a given adaptation range (Baylor et al. 1979; Krispel et al. 2003). To better understand the ability of the PVA to modulate retinal output, we evaluated the relationship between suprathreshold PVA-evoked responses as we varied NIR pulse duration or irradiance. Varying pulse duration produced a linear mPVA-evoked response that saturated at 2 msec (Figure 7A; One-way ANOVA p<0.0001; Bonferonni post hoc *p<0.05, ***p<0.001, ****p<0.0001). In contrast, the bPVA-evoked response saturated at 0.5 msec (One-way ANOVA p=0.0006; Bonferroni post hoc: ***p<0.001).

Irradiance response curves for both designs had shallow slopes over the range of irradiances tested using a 4 ms pulse duration (Figure 7B). As a result, the only significant difference was between the bPVA response at the lowest irradiance ($2.1 mW/mm^2$) when compared to the highest irradiance tested ($20.1 mW/mm^2$; One-way ANOVA p=0.0397; Bonferroni: **p<0.01). Within the ranges tested, neither PVA provides a wide range of response amplitudes, which may be a challenge for encoding a wide range of contrasts.

bPVAs provide local activation of the retina

The bPVA is designed to limit current spread, create local retinal activation and enhance spatial resolution. Figure 8Di depicts the theoretical electric field spread (related to current spread) from a monopolar versus bipolar electrode, with red areas depicting high spread and blue areas representing no/low spread. We measured the extent of local retinal activation in the SC evoked by mPVAs (n = 17 SC sites in 12 rats) and bPVAs (n = 23 SC sites in 14 rats). The recording electrode was located at an SC site near the center of the PVA activation map with robust PVA-evoked responses. PVA-evoked responses were recorded as a 0.5 mm spot (4ms pulse; $32.5 mW/mm^2$) was positioned on each of five PVA locations (center of

the PVA and four quadrants; Figure 8A). The mean mPVA-evoked peak response rarely varied significantly across stimulus location (3/17 animals; Figures 8Bi, C). In contrast, most animals (22/23) with a bPVA showed significant changes in the mean peak response across stimulus location (Figures 8 Bii, C). These results are consistent with our schematic of functional current spread in the retina (Figure 8Di) and the resulting spread of SC activation for mPVAs (Figure Dii) and bPVAs (Figure Diii). Our data are consistent with an increased current spread on the surface of the mPVA compared to the bPVA using the same reduced stimulus size (dashed line in figures Dii and Diii). Local retinal activation is likely to translate into an enhanced ability of the bPVA to provide spatially localized visual percepts.

Discussion

In this study, we compared two subretinally implanted prosthetic devices: a previously described mPVA (Chow et al. 2004) with a recently developed bPVA (Wang et al. 2012; Mathieson et al. 2012), which was designed to improve spatial activation of the retina. Our comparisons of the mPVA and the bPVA demonstrate that both interface well with the retina in the Tg S334ter-3 rat model of RP (up to 225 days of age) and produce PVA-evoked responses with thresholds well below established safety limits. Our *in vivo* characterizations provide electrophysiological support that the bPVA provides SC activation in a topographically matched area within the retinorecipient layers of the SC. In addition, we show that bPVA-evoked responses are initiated by current that stimulates the INL but not RGCs directly.

bPVA-evoked responses are mediated by the INL

Blocking retinal synaptic transmission eliminated bPVA-evoked responses in the SC. Consisent with this finding, our PVA-evoked response latencies (35 msec) are longer than latencies for direct activation of SC responses using electical stimuli delivered to the optic nerve head in cats (~14 ms; Berson 1987). Sefton (1968) reported a retina-to-SC distance in the rat of ~2 cm and RGC conduction velocities that ranged from 2.2 to 18 m/sec. Thus, the expected range of SC response latencies as a result of direct RGC activation would be ~1.1 to 9.9 ms, significantly shorter than the latencies seen here. These results are consistent with experiments that showed that both RGC responses *in vitro* and cortically evoked potentials (VEPs) *in vivo* were blocked by similar elimination of synaptic transmission (Mattheson et al. 2012; Mandel et al. 2013). Thus, the interface of the PVA with the INL should permit the remaining retinal circuitry to modulate signaling and could maintain many of the complex siganling properties of the RGC output. It should be noted, however, that NIR-evoked PVA-current will activate the On and Off retinal pathways as well as the rod and cone pathways simultaneously. This may create the need for plasticity in more central circuits to accurately interpret these artificially derived signals.

Age and duration of implantation have no effect on threshold

PVA stimulation of the retina produces similar response thresholds in the SC regardless of implantation age (P35 vs P75) or duration (50–90 vs 120–150 days). Direct electrical stimulation of Tg S334ter-3 rat RGCs in acute preparations *in vitro* also showed similar

response thresholds (Sekirnjak et al. 2009; Chan et al. 2011). Beyond 500 days, response thresholds increased in the second study (Chan et al. 2011) but this was not found in the first study (Sekirnjak et al. 2009). If thresholds were increasing at this very old age, this could reflect a change due to the significant reorganization of retinal circuitry at late stages of degeneration (Marc and Jones 2003). A stable PVA-retina interface will be required for much longer durations than explored here. Given the growing literature on the trophic benefits of low levels of electrical stimulation in RP models (Pardue et al. 2005; Morimoto et al. 2005; DeMarco et al. 2007; Okazaki et al. 2008; Ciavatta et al. 2013), it will be interesting to see if chronic stimulation (or implantation) of bPVAs positively affects reorganization and response thresholds. The results here show a viable interface between PVA and degenerate retina over more than five months. However, the ultimate utility of these prosthetics will be assessed in patients, who will require that it functions for 12+ hours per day over multiple decades.

Pixel size does not affect threshold but bPVAs had higher thresholds than mPVAs

Electrode size was previously thought to be inversely proportional to thresholds for stimulation, with smaller electrodes requiring a higher charge density (Brummer et al. 1983). When stimulating the INL with a PVA, we found that the SC response threshold in Tg S334ter-3 rats did not change as a function of pixel size (electrode size scales with pixel size), although there was a general trend for higher response thresholds with the smallest pixel size (70 μm). Similarly, pixel size did not affect threshold *in vitro* when RGCs were activated with the same subretinally placed bPVA used here (Mattheison et al. 2012). Importantly, thresholds were consistent across pixel size even though the photocollection area decreased with pixel size, indicating that the sensitivity of the devices remained the same. Consistent with our observation, perceptual thresholds were independent of electrode size (260 vs 520 μm) in human RP patients implanted epiretinally (de Balthasar et al. 2008). Further, Shyu et al. (2006) found that threshold was independent of electrode size (25 vs 125 μm) in WT rabbit retina when stimulated from the RGC side, as did Mandel et al. (2013) when recording VEPs in RCS rats using the same bPVAs described here (70, 140, 280 μm). While we did see a significantly lower threshold in mPVAs, based on our observations, this may be due to the mPVA acting functionally as a single, very large pixel (1mm).

PVA-evoked responses are topographically localized

Maintenance of a topographical representation of visual space is a critical element in prosthetic design. Our results show that subretinally placed PVAs provide an organized topographic representation across the dorsal surface of the SC, consistent with our previous work with mPVAs in RCS rats (Demarco et al. 2007) as well as retinal transplants in rat RP models (Woch et al. 2001; Sagdullaev et al. 2003). Our results enhance the understanding of the spatial localization of PVA-evoked activation and show that the bPVA design generates local activation of the retina compared to the mPVA design. The spatial extent of the PVA influence across the SC will reflect the number of RGCs recruited by the PVA stimulation as well as the size of SC neuron receptive fields (RF). In the superficial layers of the SC, RF size increases significantly with depth (up to 30 degrees; Binns and Salt 1997). Because we sought out robust PVA-evoked responses, we did not hold the depth of recording constant. This limited our ability to quantify the surface area of SC that showed PVA-evoked

activation. In the future, recording simultaneously from multiple SC depths would significantly enhance this analysis.

bPVA but not mPVA retinal stimulation produces local retinal activation

We show for the first time *in vivo* that a spatially isolated stimulus on a subretinal prosthesis (bPVA) evokes spatially localized activity in the retina. This is consistent with RGC reponses evoked *in vitro* using an even smaller (60 μm diameter) NIR spot (Matthisen et al. 2012). Together, these results are encouraging for the use of these devices in patients. At this time, poor local retinal activation appears to be a factor limiting the visual acuity achieved with prosthetic devices currently in human trials (20/560 Zrenner et al. 2011 and 20/1260 with Argus II system, Humayun et al. 2012; pixel sizes of 50×50 and 200 μm respectively). Although the devices in these trials provide limited visual acuity, this still can represent a life changing treatment, similar to cochlear implants in the deaf. The restoration of even crude spatial vision may greatly increase patient independence, allowing greater navigation in the home and community. Further advances in device design and manufacturing predict that future designs will provide the blind with much higher acuity artificial vision, as evidenced by the improvements of the bPVA design over the mPVA design presented here.

Conclusion

The results in this study show that improvements in PVA design result in local activation of the retina while maintaining thresholds below safety limits. In addition, we showed *in vivo* that transmission through the INL was required for PVA-evoked responses. This suggests that subretinally implanted PVAs can utilize the remaining retinal circuitry and its inherent signal processing. When factoring in the benefits of subretinal implantation, the photovoltaic nature of these prosthetics, and the many questions still present with other potential treatments (stem cells, genetic therapy, etc.), these devices represent an attractive treatment for photoreceptor loss.

Acknowledgments

References

Ambati J, Fowler BJ. Mechanisms of age-related macular degeneration. Neuron. 2012; 75(1):26–39. [PubMed: 22794258]

Baylor DA, Fettiplace R. Synaptic drive and impulse generation in ganglion cells of the turtle retina. J Physiol. 1979; 288:107–127. [PubMed: 469712]

Berson DM. Retinal W-cell input to the upper superficial gray layer of the cat's superior colliculus: a conduction-velocity analysis. J Neurophysiol. 1987; 58(5):1035–51. [PubMed: 3320282]

Binns KE, Salt TE. Post eye-opening maturation of visual receptive field diameters in the superior colliculus of normal- and dark-reared rats. Dev Brain Res. 1997; 99:263–266. [PubMed: 9125481]

Brummer SB, Robblee LS, Hambrecht FT. Criteria for selecting electrodes for electrical stimulation: theoretical and practical considerations. Ann N Y Acad Sci. 1983; 405:159–171. [PubMed: 6575640]

Butterwick A, Vankov A, Huie P, Freyvert Y, Palanker D. Tissue damage by pulsed electrical stimulation. IEEE Trans Biomed Eng. 2007; 54(12):2261–2267. [PubMed: 18075042]

Chan LH, Lee E-J, Humayun MS, Weiland JD. Both electrical stimulation thresholds and SMI-32-immunoreactive retinal ganglion cell density correlate with age in S334ter line 3 rat retina. J Neurophysiol. 2011; 105:2687–2697. [PubMed: 21411561]

Chen J, Makino CL, Peachey NS, Baylor DA, Simon MI. Mechanisms of rhodopsin inactivation *in vivo* as revealed by a COOH-terminal truncation mutant. Science. 1995; 267(5196):374–377. [PubMed: 7824934]

Chow AY, Pardue MT, Chow VY, Peyman GA, Liang C, Perlman JI, Peachey NS. Implantation of silicon chip microphotodiode arrays into the cat subretinal space. IEEE Trans Neural Syst Rehab Eng. 2001; 9(1):86–95.

Chow AY, Chow VY, Packo KH, Pollack JS, Peyman GA, Schuchard R. The artificial silicon retina microchip for the treatment of vision loss from retinitis pigmentosa. Arch Ophthalmol. 2004; 122(4):460–469. [PubMed: 15078662]

Chow AY, Bittner AK, Pardue MT. The Artificial Silicon Retina in retinitis pigmentosa patients (an American Opthalmological Association thesis). Trans Am Ophthalmol Soc. 2010; 108:120–154. [PubMed: 21212852]

Ciavatta VT, Mocko JA, Kim MK, Pardue MT. Subretinal electrical stimulation preserves inner retinal function in RCS rat retina. Mol Vis. 2013; 19:995–1005. [PubMed: 23687436]

Cogan SF. Neural Stimulation and Recording Electrodes. Annu Rev Biomed Eng. 2008; 10:275–309. [PubMed: 18429704]

Concepcion F, Mendez A, Chen J. The carboxyl-terminal domain is essential for rhodopsin transport in rod photoreceptors. Vision Res. 2002; 42(4):417–426. [PubMed: 11853757]

de Balthazar C, et al. Factors Affecting Perceptual Thresholds in Epiretinal Prostheses. Invest Ophthalmol Vis Sci. 2008; 49(6):2303–2314. [PubMed: 18515576]

DeMarco PJ Jr, Yarbrough GL, Yee CW, McLean GY, Sagdullaev BT, Ball SL, McCall MA. Stimulation via a subretinally placed prosthetic elicits central activity and induces a trophic effect on visual responses. Invest Ophthalmol Vis Sci. 2007; 48(2):916–926. [PubMed: 17251495]

Drager UC, Hubel DH. Topography of Visual and Somatosensory Projections to Mouse Superior Colliculus. J Neurophysiol. 1976; 39(1):91–101. [PubMed: 1249606]

Friedman DS, O'Colmain BJ, Munoz B, Tomany SC, McCarty C, de Jong PT, Nemesure B, Mitchell P, Kempen J. Prevalence of age-related macular degeneration in the United States. Arch Ophthalmol. 2004; 122(4):564–572. [PubMed: 15078675]

Gebhard JW. Thresholds of the human eye for electric stimulation by different wave forms. J Exp Psych. 1952; 44(2):132–140.

Hartong DT, Berson EL, Dryja TP. Retinitis Pigmentosa. Lancet. 2006; 358(9549):1795–1809. [PubMed: 17113430]

Humayun MS, de Juan E Jr, Weiland JD, Dagnelie G, Katona S, Greenberg R, Suzuki S. Pattern electrical stimulation of the human retina. Vision Res. 1999; 39(15):2569–2576. [PubMed: 10396625]

Humayun MS, et al. Visual perception in a blind subject with a chronic microelectronic retinal prosthesis. Vision Res. 2003; 43(24):2573–2581. [PubMed: 13129543]

Humayun MS, et al. Interim results from the international trial of Second Sight's visual prosthesis. Ophthalmology. 2012; 119(4):779–88. [PubMed: 22244176]

Jacobs GH, Fenwick JA, Williams GA. Cone-based vision of rats for ultraviolet and visible lights. J Exp Biol. 2001; 204(Pt 14):2439–2446. [PubMed: 11511659]

Jensen RJ, Rizzo JF. Activation of retinal ganglion cells in wild-type and *rd1* mice through electrical stimulation of the retinal network. Vision Res. 2001; 48:1562–1568. [PubMed: 18555890]

Jones BW, Watt CB, Frederick JM, Baehr W, Chen CK, Levine EM, Miam AH, Lavail MM, Marc RE. Retinal remodeling triggered by photoreceptor degenerations. J Comp Neurol. 2003; 464(1):1–16. [PubMed: 12866125]

Krispel CM, Chen C-K, Simon MI, Burns ME. Novel Form of Adaptation in Mouse Retinal Rods Speeds Recovery of Phototransduction. J Cell Biol. 2003; 122(6):703–712.

Kurosawa T. Selective stimulation of retinal receptors with electric currents of various forms. Tohoku J Exp Med. 1954; 62(2):195–207. [PubMed: 13291375]

Loudin JD, Simanovskii DM, Vijayraghavan K, Sramek CK, Butterwick AF, Huie P, McLean GY, Palanker DV. Optoelectronic retinal prosthesis: system design and performance. J Neural Eng. 2007; 4(1):S72–84. [PubMed: 17325419]

Loudin JD, Cogan SF, Mathieson K, Sher A, Palanker D. Photodiode circuits for retinal prostheses. IEEE Trans Biomed Circuits Syst. 2011; 5(5):468–480. [PubMed: 23852178]

Mandel Y, et al. Cortical responses elicited by photovoltaic subretinal prostheses exhibit similarities to visually evoked potentials. Nat Com. 2013; 4:1980.

Marc RE, Jones BW. Retinal remodeling in inherited photoreceptor degenerations. Mol Neurobiol. 2003; 28(2):139–147. [PubMed: 14576452]

Margalit E, Babai N, Luo J, Thoreson WB. Inner and outer retinal mechanisms engaged by epiretinal stimulation in normal and rd mice. Vis Neurosci. 2011; 28:145–154. [PubMed: 21463541]

Mathieson K, et al. Photovoltaic Retinal Prosthesis with High Pixel Density. Nature Photonics. 2012; 6(6):391–397. [PubMed: 23049619]

McGill TJ, et al. Discordant anatomical, electrophysiological, and visual behavioral profiles of retinal degeneration in rat models of retinal degenerative disease. Invest Opthalmol Vis Sci. 2012; 53(10): 6232–6244.

Morimoto T, Miyoshi T, Matsuda S, Tano Y, Fujikado T, Fukuda Y. Transcorneal electrical stimulation rescues axotomized retinal ganglion cells by activating endogenous retinal IGF-1 system. Invest Ophthalmol Vis Sci. 2005; 46(6):2147–2155. [PubMed: 15914636]

O'Hearn TM, Sadda SR, Weiland JD, Maia M, Margalit E, Humayun MS. Electrical stimulation in normal and retinal degeneration (rd1) isolated mouse retina. Vis Res. 2006; 46:3198–3204. [PubMed: 16723150]

Okazaki Y, Morimoto T, Sawai H. Parameters of optic nerve electrical stimulation affecting neuroprotection of axotomized retinal ganglion cells in adult rats. Neurosci Res. 2008; 61(2):129–135. [PubMed: 18346805]

Pardue MT, Stubbs EB Jr, Pearlman JI, Narrffstrom K, Chow AY, Peachey NS. Immunohistochemical studies of the retina following long-term implantation with subretinal microphotodiode arrays. Exp Eye Res. 2001; 73(3):333–343. [PubMed: 11520108]

Pardue MT, Phillips MJ, Yin H, Sippy BD, Webb-Wood S, Chow AY, Ball SL. Neuroprotective effect of subretinal implants in the RCS rat. Invest Ophthalmol Vis Sci. 2005; 46(2):674–682. [PubMed: 15671299]

Sagdullaev BT, Aramant RB, Seiler MJ, Woch G, McCall MA. Retinal transplantation-induced recovery of retinotectal visual function in a rodent model of retinitis pigmentosa. Invest Ophthalmol Vis Sci. 2003; 44(4):1686–1695. [PubMed: 12657610]

Sefton AJ. The innervation of the Lateral Geniculate Nucleus and Anterior Colliculus in the rat. Vision Res. 1968; 8(7):867–881. [PubMed: 5664020]

Sekirnjak C, Hulse C, Jepson LH, Hottowy P, Sher A, Dabrowski W, Litke AM, Chichilnisky EJ. Loss of responses to visual but not electrical stimulation in ganglion cells of rats with severe photoreceptor degeneration. J Neurophysiol. 2009; 102:3260–3269. [PubMed: 19726725]

Shah HA, Montezuma SR, Rizzo JF. *In vivo* electrical stimulation of rabbit retina: Effect of stimulus duration and electrical field orientation. Exp Eye Res. 2006; 83:247–254. [PubMed: 16750527]

Sha O, Kwong WH. Postnatal Developmental Changes of Vitreous and Lens Volumes in Sprague-Dawley Rats. Neuroembryology and Aging. 2006; 4:183–188.

Shyu JS, Maia M, Weiland JD, O'Hearn T, Chen SJ, Margalit E, Suzuki S, Humayun MS. Electrical stimulation in isolated rabbit retina. IEEE Trans on Neural Sys and Rehab Eng. 2006; 14(3):290–298.

Stingl K, Bartz-Schmidt KU, Gekeler F, Kusnyerik A, Sachs H, Zrenner E. Functional Outcome in Subretinal Electronic Implants Depends on Foveal Eccentricity. Invest Ophthalmol Vis Sci. 2013 (In Press).

Wang L, et al. Photovoltaic retinal prosthesis: implant fabrication and performance. J Neural Eng. 2012; 9(4):046014. [PubMed: 22791690]

Woch G, Aramant RB, Seiler MJ, Sagdullaev BT, McCall MA. Retinal transplants restore visually evoked responses in rats with photoreceptor degeneration. Invest Ophthalmol Vis Sci. 2001; 42(7): 1669–1676. [PubMed: 11381076]

Zrenner E, et al. Subretinal electronic chips allow blind patients to read letters and combine them to words. Proc Biol Sci. 2011; 278(1711):1489–97. [PubMed: 21047851]
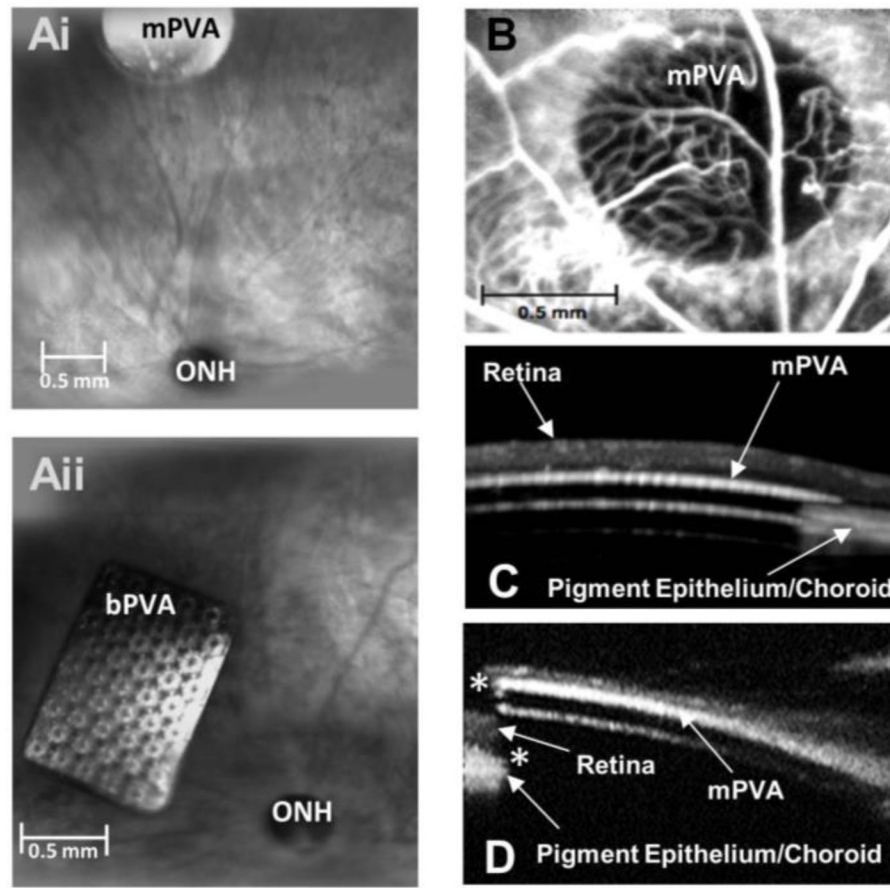
Figure 1. Retinal and vascular integrity are maintained in Tg S334ter-3 rats with subretinal PVAs

(A) Fundus images of (i) an mPVA and (ii) a medium pixel bPVA. **(B) A** representative fluorescein angiogram shows normal retinal vasculature above and beside an subretinal mPVA. **(C)** SD-OCT image of a rat retina with a subretinal mPVA. Note the close proximity of the PVA to the overlying retina. **(D)** SD-OCT image of a rat retina with a tear created by a subretinal mPVA (asterisks). We found no PVA-evoked responses in the SC of this rat. SD-OCT imaging creates a reflection artifact and the PVA appears significantly thicker than its true dimension, 20 μm. ONH=optic nerve head.
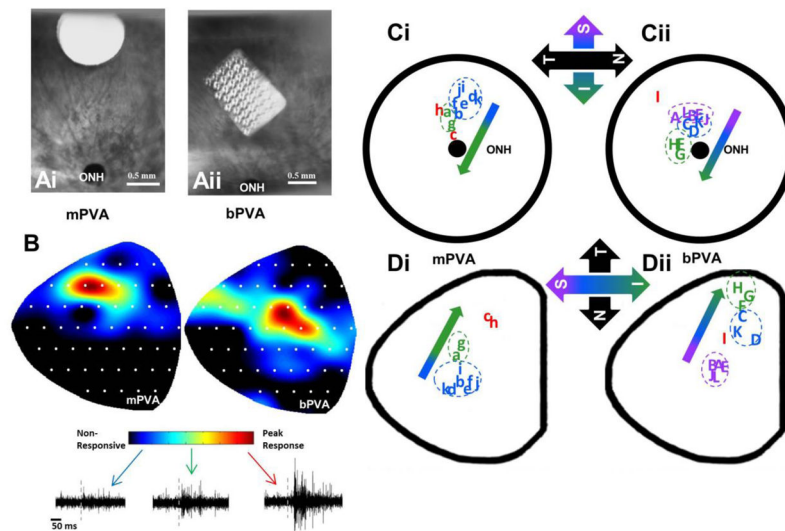
Figure 2. Representative fundus images and corresponding PVA-evoked SC activity maps
(A) Fundus images of a subretinally implanted (i) mPVA and (ii) bPVA in two rats. **(B)** PVA-evoked activity heat maps on the SC surface in the same two rats in A. On these heat maps, responsive areas are color coded. Red represents the strongest excitatory responses and blue represents the weakest responses subjective to each experiment. Black areas indicate SC locations with PVA-evoked response. Below the color scale are representative raw responses. The white dots represent the positions of the 54 recording sites across the surface of the SC. **(C)** Schematic of the retinal location of the center of each (**i**) mPVA and (**ii**) bPVA. Individual letters correspond to each rat and sites are colored coded based on proximity to the ONH. The crossed arrows show the orientation of the retina along the inferior/superior and nasal/temporal axes (T=temporal, N=nasal, S=superior, I=Inferior). **(D)** Topographic location of the center of PVA-evoked activity on the dorsal surface of the SC for mPVAs (**i**) and bPVAs (**ii**). Conventions labeling sites are the same as in **C**. Note the topographic representation of the retina in the SC causes a rotation of the axes represented by the crossed arrows. In both **C** and **D,** single headed arrows indicate the general correspondence of retinal location with PVA-evoked activity across all sites. Three sites indicated in red show poor correspondence between PVA retinal location and SC evoked activity. ONH = optic nerve head.
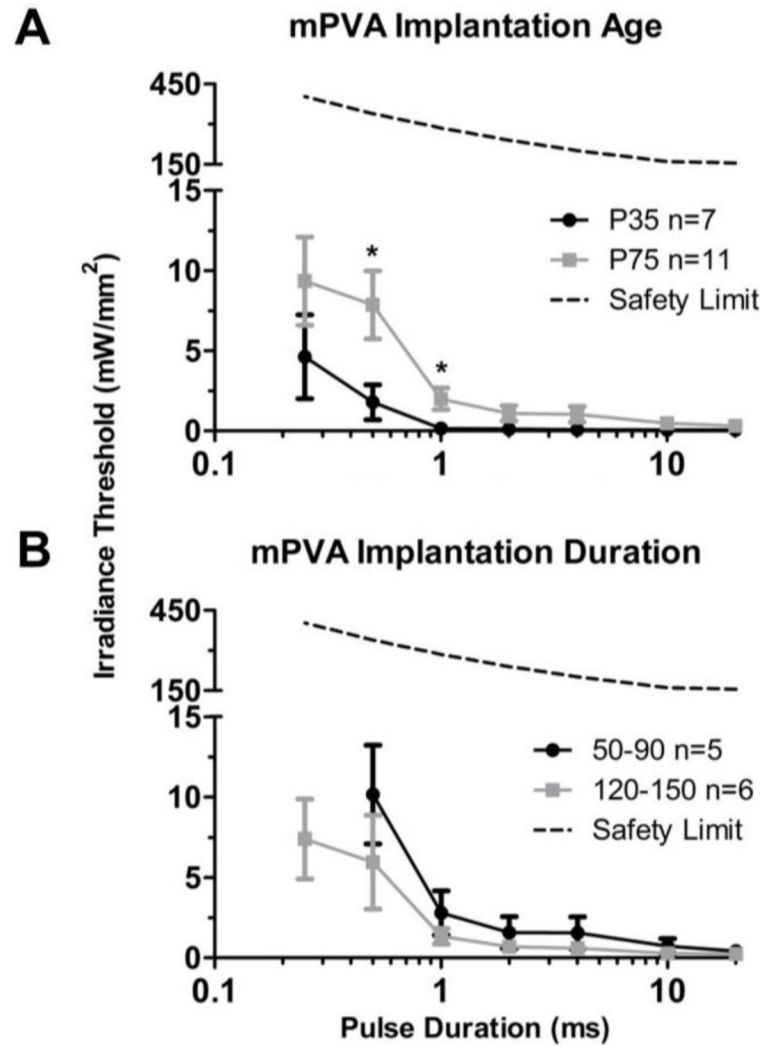
Figure 3. Response threshold is independent of implantation age and duration and well below safety limits

(**A**) mPVA-evoked response thresholds in Tg S334ter-3 rats after 120 days of implantation are similar regardless of the age of implantation, except at 0.5 and 1 ms pulse durations (P35 vs P75; t-tests at each pulse duration, with Welch's correction*p<0.05). (**B**) mPVA-evoked response thresholds in Tg S334ter-3 implanted at P75 are similar regardless of the duration of implantation (50 – 90 vs 120 – 150 days). A threshold response was evoked in only one rat implanted for 50–90 days at a pulse duration of 0.25 ms. This datum is not plotted. Dashed lines represent established safety limits of the retina to single laser pulses. Note the break in the Y-axis in both graphs.
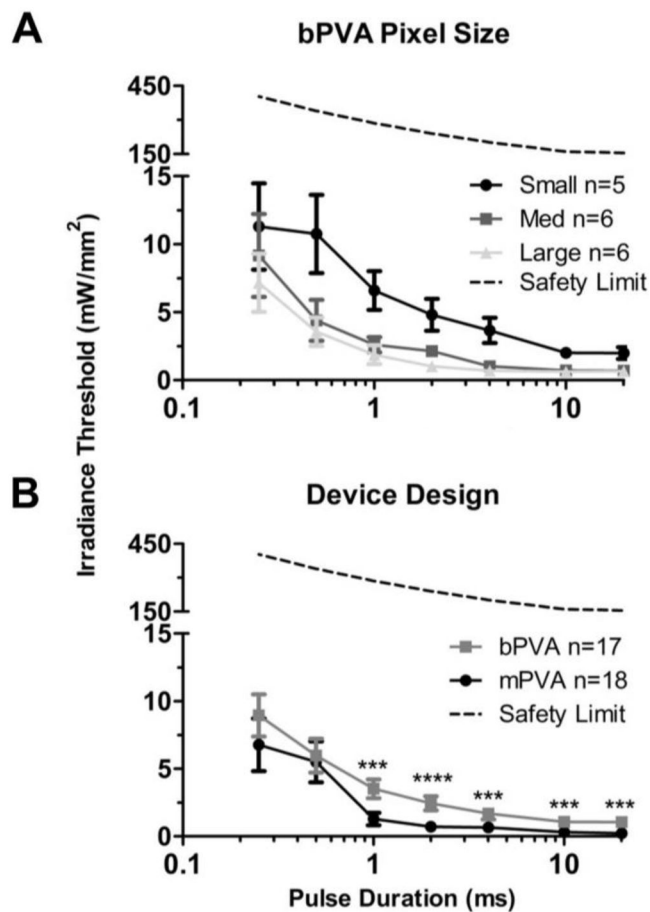
Figure 4. Response threshold is independent of bPVA pixel size but depends on PVA design
(A) bPVA pixel diameter did not significantly change threshold and all bPVAs produced thresholds below established safety limits. **(B)** bPVAs had significantly higher thresholds than mPVAs at pulse durations ≥ 1 ms (Mann-Whitney U test: ***p<0.001, ****p<0.0001). Dashed line represents safety limits for the retina to single laser pulses. Note the break in the Y-axis in both graphs and data for figure B was collapsed across all implantation ages and implantation durations.
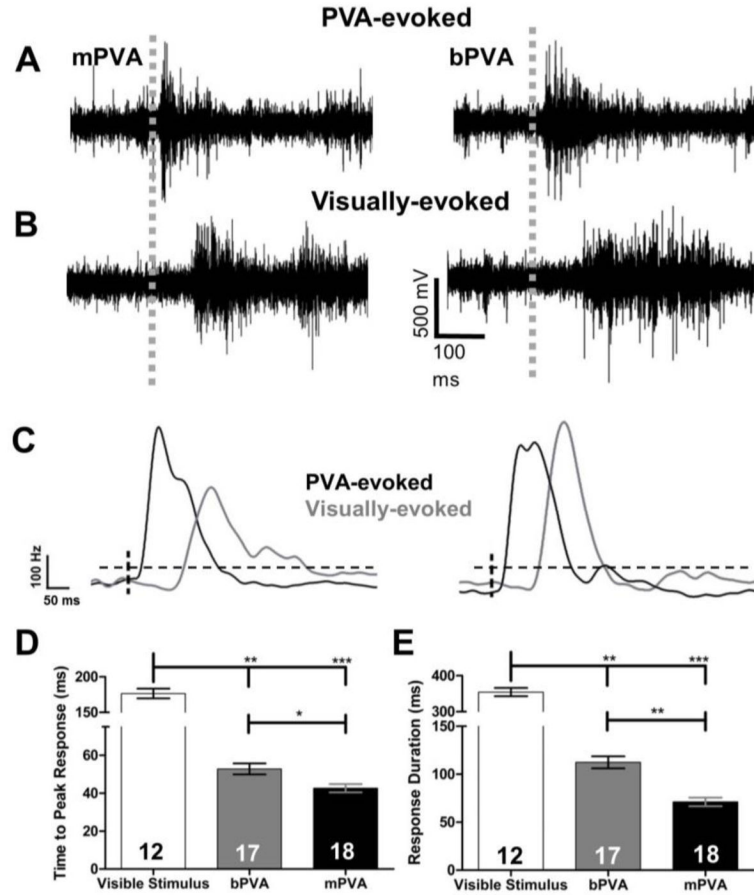
Figure 5. Implant and visually evoked response kinetics differ
(A) Representative single implant-evoked responses (IR or green laser pulse = dashed grey line) in an mPVA implanted rat (left) and a bPVA implanted rat (right) to 4 ms laser pulses (IR laser = 8.0 mW/mm^2 and green laser = 44.6 μW/mm^2). **(B)** Single visually evoked responses from the same SC location as in A. **(C)** Representative smoothed implant- (Black) or visually-evoked (grey) average responses that were used to quantify the responses (Dashed horizontal line denotes response threshold, vertical dashed line denotes the stimulus pulse). **(D)** The average time to peak of the visually-evoked response is significantly longer than either PVA-evoked average (Kruskal-Wallis p<0.0001; Dunn's Post-hoc test: *p<0.05, **p>0.01, ***p<0.001). **(E)** Similarly, the response duration of the visually-evoked response is significantly longer than either PVA-evoked response. (Kruskal-Wallis p<0.0001; Dunn's Post-hoc test: **p<0.01, ***p<0.0001). Note the break in the y-axis in both **D** and **E**.
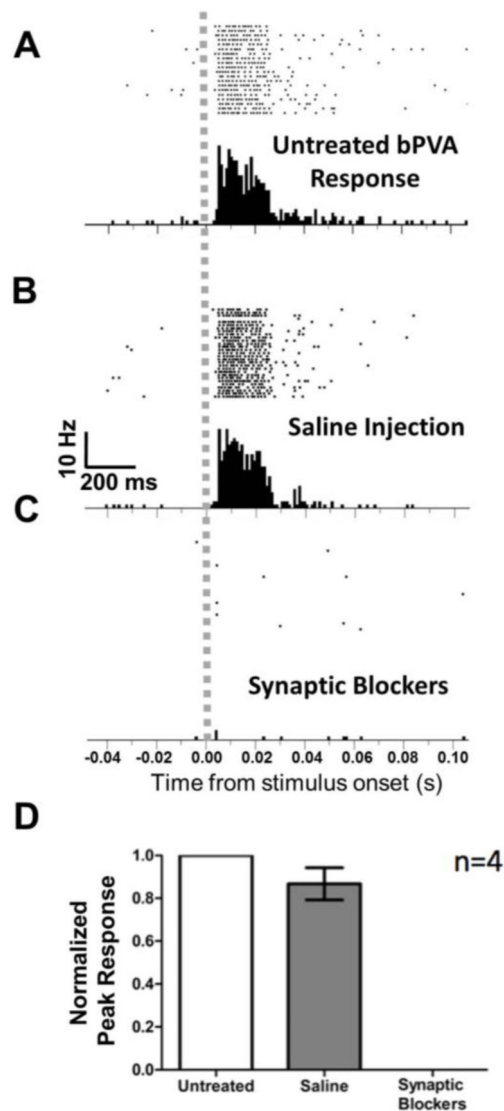
Figure 6. bPVA-evoked responses in the SC require synaptic transmission through the inner retinal circuit

(**A**) Representative raster plots and average post stimulus time histogram of bPVA-evoked responses in the SC. (**B**) After an intravitreal control injection of saline (2.5 μl), PVA-evoked responses are same (compare to **A**). (**C**) After an intravitreal injection of synaptic transmission blockers, PVA-evoked responses, as well as most spontaneous activity, are eliminated. (**D**) In all four Tg S334ter-3 rats tested, bPVA-evoked responses were eliminated after injection of synaptic transmission blockers.
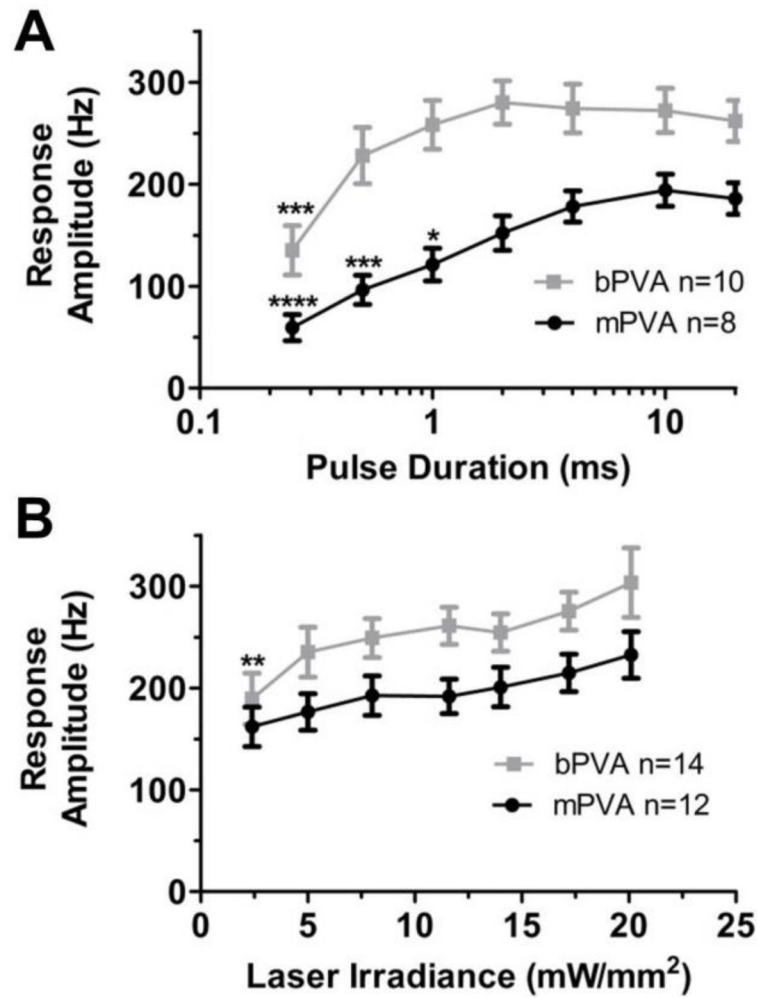
Figure 7. Response amplitudes as a function of pulse duration or laser irradiance
(A) Compared to the response amplitude of a 20 ms pulse, only the 0.25 ms response peak
was significantly lower for bPVAs (One-way ANOVA p=0.0006, Bonferroni post hoc test:
***p<0.001). mPVAs appear to have a more linear range of responses and responses at 0.25,
0.5, and 1 ms are significantly smaller than the peak response at 20 ms (One-way ANOVA
p<0.0001, Bonferroni post hoc test: *p<0.05, ***p<0.001, and ****p<0.0001) **(B)** Using a 4
ms pulse, only bPVAs stimulated at the lowest laser irradiance (2.4 mW/mm^2) showed a
significant drop in the peak response compared to the largest pulse (One-way ANOVA
p=0.0397; Bonferroni post hoc test: **p<0.01). mPVA-evoked responses were similar
across this range of irradiances (One-way ANOVA: p=0.1982). For all figures, the pulse rate
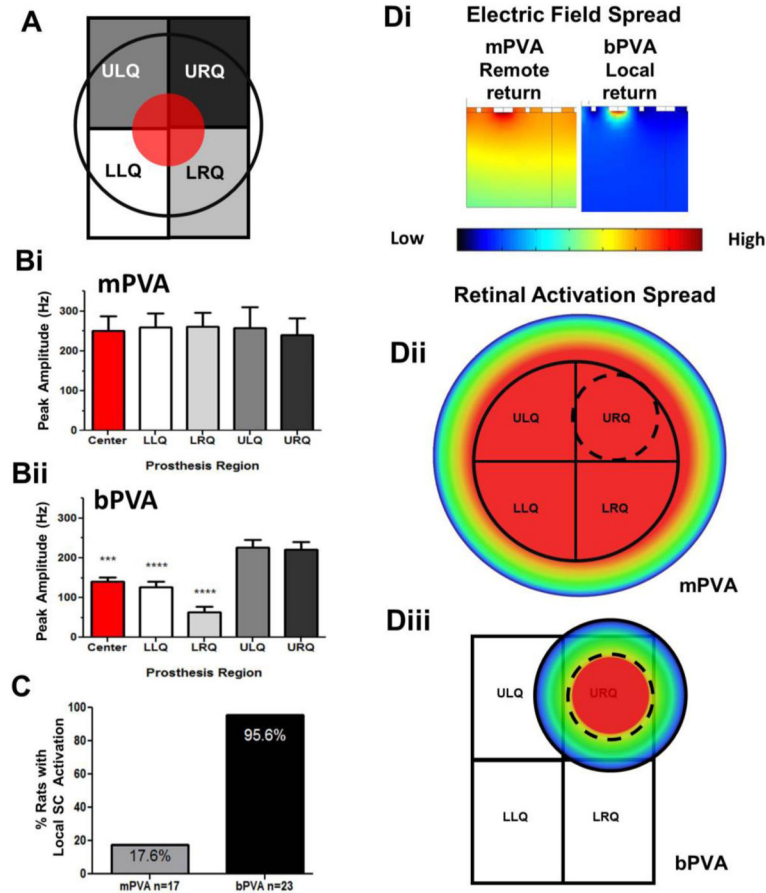was 1Hz and the spot size was 1mm.

Figure 8. bPVAs, but not mPVAs evoke spatially localized activation in the SC
(A) Schematic diagram of the stimulation approach. Each of five locations (rectangle, bPVA; large circle, mPVA) was stimulated with a NIR spot. Individual regions: upper left and right quadrants (ULQ and URQ, respectively), lower left and right quadrants (LLQ and LRQ, respectively), center red circle. **(Bi)** Representative data from a rat implanted with an mPVA, where the SC response is the same regardless of the stimulus location. **(Bii)** Representative data from a rat implanted with a bPVA, where the SC response varies significantly with stimulus location (One-way ANOVA p<0.0001; Bonferroni post hoc ***p<0.001, ****p<0.0001). **(C)** Stimulation of most bPVAs produced a response profile similar to Bii and was classified as showing local SC activation. **(D)** (i) Color coded schematic summary of mPVA and bPVA electric field spread in the retina, which is related to the current spread. (ii, iii) Schematic representations showing the spread of retinal activation when stimulating a portion of the mPVA (ii) versus the bPVA (iii). The dashed circle represents stimulus size and location relative to the PVA. Colors represent retinal activation with red areas showing high retinal activation and blue showing no/low levels of retinal activation. Figure Di (Loudin et al, 2007) is a copyright of IOP Publishing. Reproduced by permission of IOP Publishing. All rights reserved.